RSC Advances

RSC Publishing

PAPER

View Article Online
View Journal | View Issue

Characteristics of Si(111) surface with embedded C_{84} molecules

Cite this: *RSC Advances*, 2013, **3**, 9234

Chih-Pong Huang,[ab] Wan-Sheng Su,[c] Chih-Chuan Su[a] and Mon-Shu Ho*[ad]

A monolayer of fullerene molecules on Si(111) surfaces is fabricated in an ultrahigh vacuum chamber through a controlled self-assembly process. The characteristics of self-assembled Si(111) surfaces, including supramolecular structures, electronic density of states, the quantum confinement effect, field emission features, and optoelectronical properties with embedded C_{84} are determined by the use of an ultrahigh vacuum scanning probe microscope. The results revealed that such a silicon surface with embedded C_{84} has a wide band gap of ~3.4 eV, high emission efficiency and low turn-on voltage, all of which are crucial to nano-electronics, optoelectronics, and the fabrication of semiconductor carbide. The measured data derived from photoluminescence emission experiments further confirm the corresponding band gap value obtained from *I–V* curves. The theoretical results from first-principles calculations for the field enhancement factor are compared with experimental measurements.

Received 13th September 2012,
Accepted 5th April 2013

DOI: 10.1039/c3ra22151b

www.rsc.org/advances

Introduction

Carbon nanotubes and fullerenes are carbon allotropes, comprised of graphite or graphene stacks associated with linked hexagonal or pentagonal rings.[1] Composite materials developed from these have come to be considered as the next generation of nanomaterials with significant potential for solar cells, light-emitting diodes and field emission technology applications, due to their excellent properties, such as ultraviolet (UV) light emission, outstanding conductivity, superior mechanical strength, and unique chemical characteristics.[2–4] Experimental approaches as well as theoretical calculations have been employed in attempts to unravel the interaction between fullerene and various substrates.[5,6] Many researchers have elucidated the fundamental science of fullerene molecules on GaAs, highly ordered pyrolytic graphite (HOPG), and gold, silver and copper surfaces.[7,8] With regards to semiconductors, Wang *et al.* first identified bright stripes associated with C_{60} molecules on the surface of Si(100) in a study of field-ion scanning tunneling microscopy (STM).[9] Hou *et al.* identified a number of potential C_{60} adsorption sites on a Si(111)-7 × 7 surface.[10]

In addition, silicon carbide (SiC) is a leading candidate in the new generation of semiconducting materials, with important applications in a variety of fields.[11] The characteristics of these carbides include a large band gap, high thermal conductivity and stability, high saturation electron mobility, very high breakdown electronic field strength, and chemical inertness. These characteristics make SiC very attractive for use in optoelectronic devices, metal-oxide-semiconductor field-effect transistors (MOSFET), light-emitting diodes (LEDs), and high-power, high-frequency and high-temperature applications.[12,13] The field emission properties of silicon carbides have motivated many investigations due to their potential as sources of electron field emission.[14] However, high density defects, such as micropipes and dislocations, are commonly found on the surfaces of conventional silicon carbide, with potentially detrimental effects on the electronic structure, even to the point of device failure.[15] The SiC preparation process has been studied since 1960; however, the problem has yet to be resolved and remains one of the main reasons for the poor performance of these devices. Understanding the configuration of fullerene molecules on silicon surfaces is crucial to the on-going development of this technology as a replacement for silicon carbide as a semiconducting material.

In this study, a silicon surface is fabricated with an embedded monolayer of C_{84} as a successor to silicon carbide materials. The supramolecular structures and the orientations of C_{84} molecules on Si(111)-7 × 7 surfaces are elucidated in detail by ultrahigh vacuum scanning probe microscopy (UHV-SPM).[16,17] The self-assembled layers of C_{84} on the Si(111) surfaces are fabricated using special annealing treatments. Interactions between fullerenes and the surrounding silicon atoms are discussed. The corresponding electronic properties, such as electronic density of states, energy difference between the highest occupied molecular orbital (HOMO) and the lowest

[a]*Department of Physics, National Chung Hsing University, Taichung 402, Taiwan E-mail: msho@dragon.nchu.edu.tw; Fax: +886 4 22862534; Tel: +886 4 22840427 ext. 519*
[b]*Physics Division, Institute of Nuclear Energy Research, Taoyuan County 325, Taiwan*
[c]*National Center for High-Performance Computing, Tainan 741, Taiwan*
[d]*Institutes of Nanoscience, National Chung Hsing University, Taichung 402, Taiwan*

unoccupied molecular orbital (LUMO) levels which is regarded as band gap energy, and field emission characteristics are estimated from *I–V* and F–N (Fowler–Nordheim) measurements.[18] The optoelectronic properties, determined from photoluminescence (PL) emission measurements, are further discussed. As the devices that are currently produced by the silicon-based electronics industry are approaching their physical limits, finding alternative materials is an urgent priority. This work develops a material with many advantages over conventional silicon carbides and without porous defects, which can therefore be used as a substitute in optoelectronic and electronic devices. Accordingly, silicon surfaces with embedded fullerenes are expected to contribute greatly to current nanoscience research.

Experimental

Sample preparation

A variable-temperature SPM (JSPM-4500A), comprising a scanning tunneling microscope (STM) and an atomic force microscope (AFM), was utilized in all experiments in an UHV chamber with a base pressure of around 7×10^{-9} Pa. The STM tip is an electrochemically etched tungsten tip with a diameter of around 50–100 nanometers at its very end (apex). It is bombarded for 10 min with hot electrons to remove most impurities. The tip is further cleaned and the structure is reshaped by applying high voltage, which is a standard but somewhat extreme method to change the tip shape. Our procedure causes tips to reform with only a couple of atoms on the apex in order to fit the STM requirements.[19,20] All the STM images were captured in constant current mode with a tunneling current of around 0.1 nA. The supramolecular structures and the orientations of the fullerenes were observed under various applied sample biases. The specimens were n-type Si(111) wafers with a resistivity of 0.05–0.1 Ω cm. A clean Si(111) substrate was prepared by degassing a sample at 600 °C for many hours to remove surface contaminations; flashing it to 1250 °C, and either slowly cooling it to produce 7×7 reconstructions, or quenching it to room temperature to form disordered regions. The defect densities of the 7×7 surfaces were maintained under ~1% to prevent any influence of the fullerene adsorption on the substrate. C_{84} molecules were chosen for presentation in this paper over C_{60}, because oval-shaped C_{84} possesses a larger height-to-diameter ratio, approximately 1.3 times that of the roughly spherical C_{60}, in free space. Other fullerenes, which were larger than C_{84} molecules, offer structural possibilities but are difficult to purify. Furthermore, the proposed self-assembly mechanism is difficult to apply to very large fullerenes. In the experiment, 98%-pure C_{84} (Aldrich Corp., Fullerene – C_{84}) powder was used. The base pressure was maintained at under 5×10^{-8} Pa during deposition. Fullerene molecules were deposited onto the silicon substrate at 650 °C from a pyrolytic boron nitride (PBN) crucible in a K-cell evaporator (Vacweld, Miniature K-cell). The silicon substrate was pre-annealed at 800 °C for 30 min. A hexagonal close-packed structure of C_{84} arrays gradually formed on the surface during annealing.

***I–V* characteristics and PL emission measurements.** The *I–V* characteristics and local field emission properties of the silicon surface with embedded C_{84} were examined using an UHV-STM at room temperature. The spacing between the STM tip and the substrate was controlled at several nanometers. The *I–V* curve reveals the interaction between the discrete molecular levels and the charging effects of the C_{84} molecules. The differential conductance (d*I*/d*V*) spectrum was transformed to total conductance. The tip effect was studied using various scanning speeds and different bias voltages and tunneling currents. The optoelectronical properties were obtained from measurements of PL emission experiments using a He–Cd laser source at 325 nm at room temperature.

Field enhancement factor calculations. The calculations were done within the framework of the local density approximation (LDA)[21] using the Ceperley–Alder form of exchange–correlation functional[22] and the highly accurate projected augmented wave (PAW) method[23,24] with a plane wave cutoff of 400 eV, as implemented in the Vienna *Ab initio* Simulation Package (VASP).[25] A supercell geometry was adopted and the C_{84} molecules without a Si(111) substrate support (due to limited computational resources) were arranged in a hexagonal close-packed array with a center-to-center distance of 11.7 Å, a value derived from experimental results. The lattice constant of the supercell along the *z*-axis is given by $L + Dv$, where L is the length of the C_{84} molecule and Dv is the vacuum thickness along the *z*-axis, which is set to 20 Å. Fig. 1 depicts the structural model. For Brillouin-zone integrations, the k-point sampling was set to $4 \times 4 \times 1$. All atoms were fully relaxed until the residual force on each atom was less than 0.02 eV $Å^{-1}$.

In order to study the enhancement factor β property, we impose an *E*-field by applying a classical dipole sheet at the middle of the vacuum region in the *z*-direction. The dipole correction is included in the calculations and the distortions in atomic structures induced by the external field are neglected. The value of β is dimensionless and can be calculated directly from the ratio of the maximum value of E_{loc}, on the tube axis near its end, to E_{app}, where E_{loc} and E_{app} are terms for the local electric field and the applied electric field, respectively. The magnitude of E_{loc} is the derivative of the Coulomb potential energy difference caused by the presence of an applied field with respect to the position.[26]

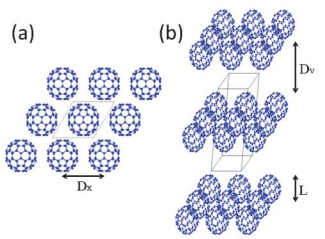

Fig. 1 Models of the C_{84} molecules with Si(111) substrate removed, arranged in a hexagonal close-packed array in (a) top and (b) side views.

Results and discussion

With the very low coverage deposition of about ~0.011 C_{84} molecules per 7 × 7 half-unit-cell (HUC), the supramolecular features of the C_{84} molecules, in particular unit cells at room temperature, have been revealed in our previous work.[16] At room temperature, C_{84} was adsorbed at eight kinds of sites on the Si(111)-7 × 7 surfaces. At five of them, horizontal adsorption in the 7 × 7 halves and at the corner holes occurred.[16] At the other three, vertical deposition on the 7 × 7 surfaces occurred in a faulted half, an unfaulted half and a corner hole. The relevant illustrations for these three are given in Fig. 2 (a–c). The supramolecular structure, orientation and profile of vertically deposited C_{84} molecules were also discussed in our previous work.[16] Based on the STM results, C_{84} molecules prefer to remain in the 7 × 7 halves rather than the corner holes. The ratio of C_{84} molecules that stay in the 7 × 7 halves to those in the corner holes is about 11 : 1. A statistical study of over 600 adsorption sites indicated that 87.9% of C_{84} molecules were horizontally deposited on the 7 × 7 surfaces and only 12.1% were adsorbed vertically. Such an investigation also estimated the variation in the activation energy of C_{84} molecules among various adsorption sites. Based on an Arrhenius analysis, the activation energy varied among the eight sites by around 10^{-2} eV, implying that the supramolecular features of C_{84} molecules could be gently modified by slightly heating the Si(111)-7 × 7 surface. The cage diameter of the C_{84} molecule in free space is found to be ~7 Å × 9 Å. The surface feature of C_{84} molecules on the 7 × 7 surfaces showed approximately 5 Å on the profile analysis, which is smaller than the size of C_{84} in free space. These results indicate that the C_{84} molecules that were embedded on silicon surfaces underwent relaxation. Moreover, the surrounding Si adatoms appeared darker than usual in the STM images under a negative sample bias, probably because charge transfer occurred from surface Si atoms to C_{84} molecules.[27]

Through a special annealing process, 7 × 7 reconstructions were destroyed before the C_{84} molecules aggregated into hexagonal close-packed C_{84} clusters on the Si(111) surface. The structure and nucleation mechanism, confirmed by the STM images, are important in the self-assembly process. The preferred energy of adsorption in the disordered regions containing 1 × 1, 2 × 2, c(4 × 2) and $\sqrt{3} \times \sqrt{3}$ structures is much less than that on 7 × 7 surfaces. The Si(111)-3 × 3–C_{84} super-lattice structure was identified as having a nearby 7 × 7 structure on the Si(111) surface (Fig. 3). The STM images also revealed that C_{84} molecules preferentially and vertically aggregated on a disordered Si(111) surface although many C_{84} molecules can be deposited on the Si(111)-7 × 7 surface in many orientations.

The layer-by-layer growth was studied and the C_{84} molecules were highly uniformly distributed on the silicon substrate following the special annealing process. Fig. 4(a) and (b) present a flat, self-assembled single and double layers of C_{84} molecules, respectively, on the Si(111)-disordered surface. Fig. 4(c) presents a close view of a C_{84} molecule and reveals that most of the C_{84} molecules are perpendicular to the

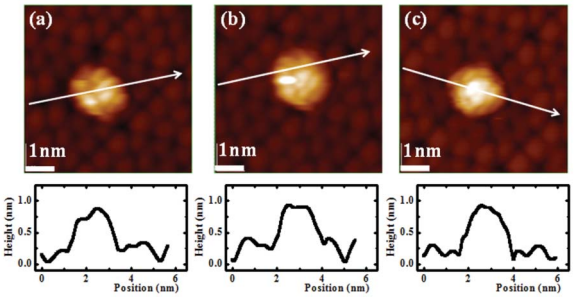

Fig. 2 STM images with analysis of profiles of a C_{84} molecule adsorbed vertically in (a) a faulted half, (b) an unfaulted half and (c) a corner hole on the Si(111)-7 × 7 surface, respectively.

Si(111) surface. The side view diagram of the Si substrate with embedded C_{84} is depicted in Fig. 4(d). In addition, a schematic diagram of top and side views of possible atomic structures of the C_{84}-embedded Si(111)-1 × 1 surface is shown in Fig. 4(e). The measured profiles in Fig. 4(a) and (b) indicate that the surface feature and spacing are approximately 6.5 and 11.7 Å, respectively, for a single C_{84} layer, and 4.1, 3.6 and 11.4 Å for double C_{84} layers. These findings indicate that C_{84} was preferentially adsorbed in the holes of the first layer because of the lower adsorption energy. The stacking feature in the C_{84} multi-layer deposition was smaller than in the single-layer deposition. Higher temperature annealing (above ~900 °C) destroyed the caged structure of the C_{84} molecules and strengthened the C–Si bonds. The carbon silicide then began to form roughly on the Si(111) surface.

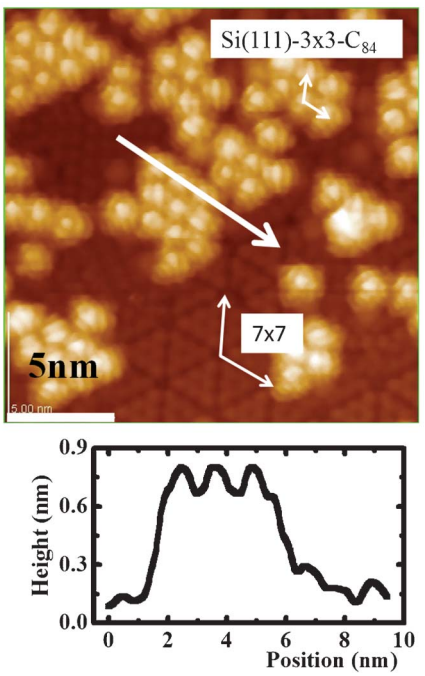

Fig. 3 STM images with analysis of profile of Si(111)-3 × 3–C_{84} super-lattice surface on self-assembled surfaces.

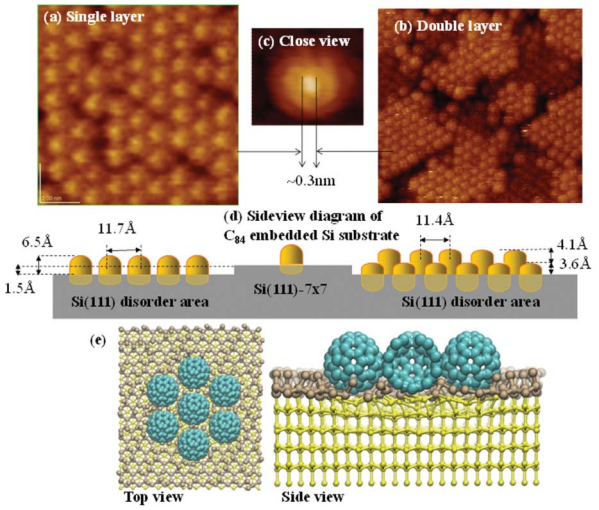

Fig. 4 STM images of (a) single and (b) double layer C_{84}-embedded Si(111) surface. (c) A close view of a C_{84} molecule on the self-assembled surface. (d) Illustration of self-assembled C_{84}-embedded Si(111) surface. (e) A schematic diagram of top and side views of possible atomic structures of the C_{84}-embedded Si(111)-1 × 1 surface.

Fig. 5(a) plots the conductance dI/dV as a function of applied voltage, which corresponds to the local electronic states of the substrate, for four cases: single C_{84} molecules, small-clusters of 7 to 13 C_{84} molecules, island-clusters with a hexagonal C_{84} arrangement of ~10 nm × 10 nm and a single layer of self-assembled C_{84} substrate, respectively. The curves indicate that the silicon substrate with either small amounts of C_{84} molecules or a C_{84} self-assembled layer exhibits semiconductor properties. In addition, the energy difference between the HOMO and LUMO levels of the Si surface with clean 7 × 7 surfaces, single C_{84} molecules, small-clusters, island-clusters and the single self-assembled C_{84} layer, were approximately 1.4 ± 0.2, 1.6 ± 0.4, 2.1 ± 0.3, 2.8 ± 0.3 and 3.4 ± 0.6 eV, respectively. The error bars shown in Fig. 5(b) were obtained from the standard deviations of over 50 measurements for each data point. The smaller energy difference between the HOMO and LUMO levels of single C_{84} molecules results from the support of the silicon substrate. As more C_{84} molecules aggregate together and form larger size clusters, the energy difference between the HOMO and LUMO levels increases considerably. The relevant conductance spectra of self-assembled C_{84} substrate shown in Fig. 5(b) have many prominent peaks, which corresponded to various quantum well states. These results confirm that such a silicon substrate with embedded self-assembled C_{84} has a larger band gap for use in optoelectronic applications as compared to silicon (1.1 eV), GaAs (1.42 eV) and SiC (2.3–3.2 eV).[28]

With more C_{84} deposition, the C_{84} molecules start to occupy the holes of the first layer and aggregate to again form island-like clusters on the single layer C_{84}-embedded Si substrate as shown in Fig. 6(a). The island-clusters were around 10 nm × 10 nm and were uniformly distributed on the surface. A close view of these island-clusters, taken by STM, revealed that the individual C_{84} molecules remained on the clusters (Fig. 6(b)). The dI/dV as a function of voltage for island-like clusters is plotted in Fig. 6(c). The energy difference between the HOMO and LUMO levels for those clusters was about 2.9 ± 0.5 eV, which was close to the value obtained from island-clusters supported by a silicon surface. Again, the fine peaks shown in the conductance spectra in Fig. 5(a) and 6(c) were attributed to quantum confinement.

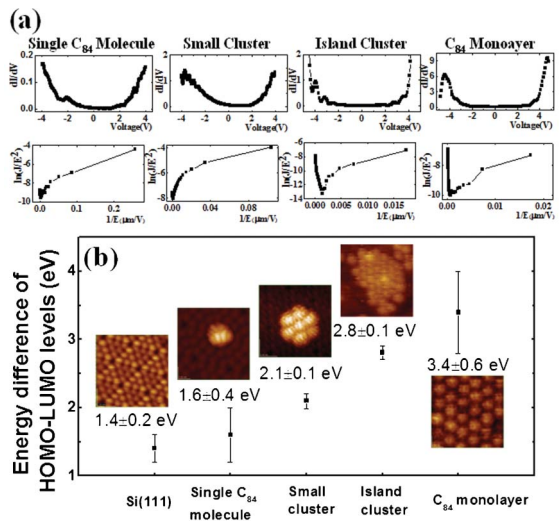

Fig. 5 (a) Current *versus* voltage curves and corresponding F–N plots for single C_{84} molecules, small-clusters, island-clusters and a single layer of self-assembled C_{84} substrate, determined by UHV-STM. (b) The energy difference between the HOMO and LUMO levels of the Si surface for clean 7 × 7 surfaces, single C_{84} molecules, small-clusters, island-clusters and a single layer of self-assembled C_{84}.

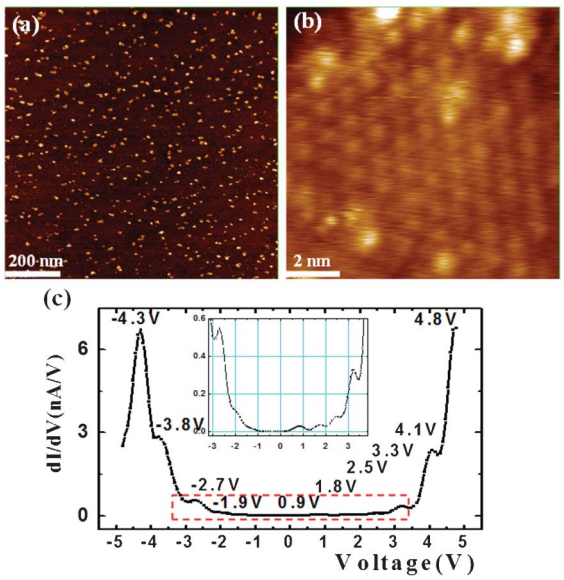

Fig. 6 STM images of (a) C_{84}-embedded substrate with island-clusters, and (b) close view of island-clusters. (c) Conductance spectrum of island-like clusters on C_{84}-embedded surfaces. The inset is an enlargement of the area marked by the red dashed box.

The presented *I–V* curve is also transformed into a plot of current density as a function of the electric field (V/d) plot, as shown in Fig. 5(a). The V here is the applied voltage and d represents the distance between the STM tip and the silicon substrate with embedded C_{84}, which is about 1 nm. A low turn-on electric field (E_{on}) of 540, 401, 460 and 1363 V μm^{-1} was measured for the single C_{84} molecule, small-clusters, island-clusters and a single layer of self-assembled C_{84} hereof on the substrate, respectively, at a current density (J_{on}) of 10^8 μA cm^{-2}. All four corresponding F–N plots in Fig. 5(a), which capture the field emission characteristics of the substrate, satisfy linear relations. Many parameters influence the field emission characteristics,[29] including the work function, emission area, geometry, structure, aspect ratio, and shielding of the substrate by the neighboring emitters. Generally, a higher emission current density can be generated by a material with a lower work function. However, not all materials that have low work functions are perfect emitters. The geometrical field enhancement factor, β, which plays an important role in dominating the field emission efficiency, can be derived from a calculation of the slope of the F–N plot. In this investigation, the work function of the silicon substrate with embedded C_{84} is about 5 eV, near that of graphite.[30] Based on the slope of the F–N plot, the field enhancement factor β in the UHV-STM system was thus estimated to be around 59.2, 46.9, 6 and 2.9 for the single C_{84} molecule, small-clusters, island-clusters and the single layer of silicon substrate with self-assembled C_{84}, respectively. As is widely assumed, a higher height-to-diameter ratio favors the field emission.[31] Since C_{84} was oval-shaped with a height-to-diameter ratio of around 1.3 compared to the spherical C_{60}, such an expanded ratio improves the field emission characteristics, with the diameter of the top of a C_{84} molecule on a Si surface being only 0.3 nm (Fig. 4(c)). The spacing-to-height ratio of the Si(111) substrate with embedded C_{84} is approximately 1.8, which is close to the ideal value of $\sim$2 for field emission in simulations of patterned carbon nanotube films.[32,33]

The field enhancement factor β is estimated to be around 2.9 by the UHV-STM system. This finding can be attributed to the fact that the geometry and diameter of the STM tip (anode) are similar to those of the C_{84} molecules (cathode). The anode and cathode resemble parallel plates at an extremely small distance from each other. In this investigation, β is computed directly from the ratio of the maximum value of the local electric field to the applied electric field for the C_{84} molecule without a silicon substrate based on the density functional theory. The resulting β of approximately 1.5 is of the same order as the experimental value of 2.9, attributable to the field screening effect that is associated with the proximity of neighboring nanostructures.[34] Note that the discrepancy is likely due to the fact that our calculations do not consider a silicon substrate effect; however, were they to consider that effect, the result should be close to 2.9. When the sample was thinly covered, the field enhancement factor β of the self-assembled C_{84} layers of the Si substrate with embedded fullerene was rather large and the turn on field was relatively small. The morphology of each sample of the silicon surface with embedded C_{84} was re-examined after field emission operations. The STM images reveal that the Si(111) surface with embedded self-assembled C_{84} has excellent electronic properties after many field emission measurements, and that the arrangement of the C_{84} molecules on the silicon surface change very little.

The optoelectronic properties were obtained from PL emission measurement using a He–Cd laser source at 325 nm at room temperature, as shown in Fig. 7. The PL peaks, which are related to electronic transitions between conductive and valence bands, can be used to confirm the band gap from the *I–V* curve. The band gap energy of SiC of various polytypes, such as 3C, 6H and 4H, is reported to be 2.69 eV.[28] The spectra indicated that the Si substrate with high-coverage embedded C_{84} emitted UV and near-UV light at 3.4, 2.98 and 2.67 eV, corresponding to the HOMO–LUMO energy differences for a single layer C_{84}-embedded Si substrate, for 10 nm $\times$ 10 nm island-clusters with a single layer C_{84}-embedded Si substrate, and for SiC interaction between C_{84}-embedded Si substrates. Full widths at half-maxima (FWHM) of 0.20, 0.31 and 0.68 eV were fitted to Gaussian curves of the 3.4, 2.98 and 2.67 eV peaks, respectively. Unlike those of the other SiC polytypes, they are determined by the substrate support and the quantum size effect. The latter causes smaller particles to have larger band gap energies because the motions of electrons and holes in a small space are quantized. As such, the band gap energy of quantum dots increases as their size decreases because their electronic properties depend strongly on the crystalline size.[35] In this study, the C_{84} molecules and island-like clusters serve as quantum dots on the Si surfaces and on the single layer C_{84}-embedded Si substrate, respectively. The fine peaks in the PL measurements are 72.3 $\pm$ 9.3 and 51.2 $\pm$ 5.7 meV for the primary 3.4 and 2.98 eV peaks. These spectra represent the quantum states of a single layer C_{84}-embedded Si surface and island-like clusters on a single layer C_{84}-embedded Si substrate, respectively. The photoluminescence efficiency of the self-assembled C_{84} exceeds that of crystalline silicon and silicon carbide. These results should prove useful in developing optoelectronic applications in the UV light emission range.

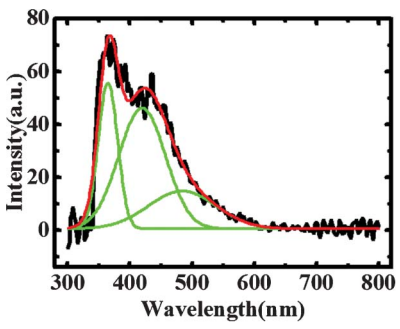

Fig. 7 PL spectrum of single layers of self-assembled C_{84} substrate.

Conclusions

The supramolecular nanostructures of Si(111) surfaces with embedded self-assembled C_{84} were studied using UHV-STM. Such a system not only has advantages over conventional silicon carbide devices, but also has no porous defects. This investigation also determined the electronic density of states and the optoelectronic properties of the Si(111) surfaces with embedded C_{84}. The field emission properties of single C_{84} molecules, small clusters, island-clusters and a single layer of self-assembled C_{84} substrate were obtained from *I–V* characteristics. The electron field emission was stable for a period, revealing a stable interaction between fullerene molecules and the silicon substrate. Calculations from the first-principles method were compared with experimental results. The results of this study can help to improve the fabrication of optoelectronic devices and may serve as a replacement for semiconductor carbide.

Acknowledgements

The authors would like to thank the National Science Council of Taiwan, for financially supporting this research under Contract Nos NSC99-2112-M-005-002-NY3 and NSC-101-2112-M-492-001-MY3 (WSS). Support from the National Centers for Theoretical Sciences (South) and High-performance Computing of Taiwan in providing huge computing resources to facilitate this research are also gratefully acknowledged.

References

1 H. W. Kroto, J. R. Heath, S. C. O'Brien, R. F. Curl and R. E. Smalley, *Nature*, 1985, **318**, 162–163.
2 Z. K. Tang, L. Y. Zhang, N. Wang, X. X. Zhang, G. H. Wen, G. D. Li and J. N. Wang, *et al.*, *Science*, 2001, **292**, 2462–2465.
3 S. Iijima, *Phys. B*, 2002, **323**, 1–5.
4 F. Diederich, R. Ettl, Y. Rubin, R. L. Whetten, R. Beck, M. Alvarez and S. Anz, *et al.*, *Science*, 1991, **252**, 548–551.
5 I. D. Hands, J. L. Dunn and C. A. Bates, *Phys. Rev. B: Condens. Matter Mater. Phys.*, 2010, **81**, 205440–205452.
6 J. I. Pascual, J. Gómez-Herrero, C. Rogero, A. M. Baró, D. Sánchez-Portal and E. Artacho, *et al.*, *Chem. Phys. Lett.*, 2000, **321**, 78–82.
7 Y. Z. Li, J. C. Patrin, M. Chander, J. H. Weaver, L. P. F. Chibante and R. E. Smalley, *Science*, 1991, **252**, 547–548.
8 Y. Nakamura, F. Kagawa, K. Kasai, Y. Mera and K. Maeda, *Appl. Phys. Lett.*, 2004, **85**, 5242–5244.
9 X. D. Wang, T. Hashizume, H. Shinohara, Y. Saito, Y. Nishina and T. Sakurai, *Phys. Rev. B: Condens. Matter*, 1993, **47**, 15923–15930.
10 J. G. Hou, J. L. Yang, H. Q. Wang, Q. X. Li, C. G. Zeng and H. Lin, *et al.*, *Phys. Rev. Lett.*, 1999, **83**, 3001–3004.
11 J. Y. Fan, X. L. Wu and Paul K. Chu, *Prog. Mater. Sci.*, 2006, **51**, 983–1031.
12 J. Xu, J. Mei, Y. Rui, D. Chen, Z. Cen and W. Li, *et al.*, *J. Non-Cryst. Solids*, 2006, **352**, 1398–1401.
13 H. W. Shim, K. C. Kim, Y. H. Seo, K. S. Nahm, E.-K. Suh and H. J. Lee, *et al.*, *Appl. Phys. Lett.*, 1997, **70**, 1757–1759.
14 Z. S. Wu, S. Z. Deng, N. S. Xu, J. Chen, J. Zhou and J. Chen, *Appl. Phys. Lett.*, 2002, **80**, 3829–3831.
15 P. G. Neudeck and J. A. Powell, *IEEE Electron Device Lett.*, 1994, **15**, 63–65.
16 C. P. Huang, C. C. Su and M. S. Ho, *Appl. Surf. Sci.*, 2008, **254**, 7712–7717.
17 C. P. Huang, C. F. Hsu and M. S. Ho, *J. Nanosci. Nanotechnol.*, 2010, **10**, 7145–7148.
18 C. P. Huang, C. C. Su, W. S. Su, C. F. Hsu and M. S. Ho, *Appl. Phys. Lett.*, 2010, **97**, 061908–061910.
19 G. Binnig, *et al.*, *Rev. Mod. Phys.*, 1999, **71**, S324–S330.
20 I. Ekvall, E. Wahlström, D. Claesson, H. Olin and E. Olsson, *Meas. Sci. Technol.*, 1999, **10**, 11–18.
21 W. Kohn and L. J. Sham, *Phys. Rev.*, 1965, **140**, A1133–A1138.
22 F. Manghi, G. Riegler, C. M. Bertoni, C. Calandra and G. B. Bachelet, *Phys. Rev. B*, 1983, **28**, 6157–6160.
23 P. E. Blöchl, *Phys. Rev. B: Condens. Matter*, 1994, **50**, 17953–17979.
24 G. Kresse and D. Joubert, *Phys. Rev. B: Condens. Matter Mater. Phys.*, 1999, **59**, 1758–1775.
25 G. Kresse and J. Furthmüller, *Comput. Mater. Sci.*, 1996, **6**, 15–50.
26 W. S. Su, F. C. Chuang, T. H. Cho and T. C. Leung, *J. Appl. Phys.*, 2009, **106**, 014301–014304.
27 C.-P. Cheng, T.-W. Pi, C.-P. Ouyang and J.-F. Wen, *J. Vac. Sci. Technol., B*, 2005, **23**, 1018–1023.
28 Otfried Madelung, in *Semiconductors: Data handbook*, Springer Verlag, Berlin, 3rd edn, 2004.
29 H. Zhang, P. X. Feng, P. Jin, V. I. Makarov, L. Fonseca and G. Morell, *et al.*, *Appl. Phys. Lett.*, 2009, **95**, 061906–061908.
30 J. W. Gadzuk and E. W. Plummer, *Rev. Mod. Phys.*, 1973, **45**, 487–548.
31 W. Z. Wang, B. Q. Zeng, J. Yang, B. Poudel, J. Y. Huang, M. J. Naughton and Z. F. Ren, *Adv. Mater.*, 2006, **18**, 3275–3278.
32 Y. L. Chueh, L. J. Chou, S. L. Cheng, J. H. He, W. W. Wu and L. J. Chen, *Appl. Phys. Lett.*, 2005, **86**, 133112–133114.
33 J. M. Bonard, N. Weiss, H. Kind, T. Stockli, L. Forro and K. Kern, *et al.*, *Adv. Mater.*, 2001, **13**, 184–188.
34 W. I. Milne, K. B. K. Teo, G. A. J. Amaratunga, P. Legagneux, L. Gangloff and J. P. Schnell, *et al.*, *J. Mater. Chem.*, 2004, **14**, 933–943.
35 D. H. Feng, Z. Z. Xu, T. Q. Jia, X. X. Li and S. Q. Gong, *Phys. Rev. B: Condens. Matter*, 2003, **68**, 035334–035340.